Received: 30 July 2018 | Revised: 15 February 2019 | Accepted: 20 February 2019

DOI: 10.1002/jcp.28494

ORIGINAL RESEARCH ARTICLE

WILEY Journal of Cellular Physiology

Human umbilical artery endothelial cells from Large-for-Gestational-Age newborn have increased antioxidant efficiency and gene expression

Ivo Carrasco-Wong[1*] | Cherie Hernández[2] | Carlos Jara-Gutiérrez[3] | Omar Porras[4] | Paola Casanello[2,5]

[1]Department of Cellular and Molecular Biology, Cell & Molecular Biology PhD Program, Faculty of Biological Sciences, Pontificia Universidad Católica de Chile, Santiago, Chile

[2]Department of Obstetrics, School of Medicine, Pontificia Universidad Católica de Chile, Santiago, Chile

[3]Centro de Investigaciones Biomédicas (CIB), Laboratorio de Estrés Oxidativo, Facultad de Medicina, Universidad de Valparaíso, Valparaíso, Chile

[4]Unidad de Nutrición Básica, Instituto de Nutrición y Tecnologí, Instituto de Nutrición y Tecnología de los Alimentos (INTA), Universidad de Chile, Santiago, Chile

[5]Department of Neonatology, School of Medicine, Pontificia Universidad Católica de Chile, Santiago, Chile

Correspondence
Ivo Carrasco MSc, PhD Program in Cell & Molecular Biology, Faculty of Biological Sciences, Pontificia Universidad Católica de Chile, Avda. Libertador Bernardo O'Higgins 340, Santiago, Chile.
Email: icarrasco@uc.cl
Dr. Paola Casanello, Department Obstetrics, Department of Neonatology, School of Medicine, Pontificia Universidad Católica de Chile, Marcoleta 391, Santiago, Chile.
Email: pcasane@uc.cl

Current address
*Biomedical Research Center, School of Medicine, Universidad de Valparaíso, Valparaíso, Chile.

Funding information
Comisión Nacional de Investigación Científica y Tecnológica, Grant/Award Numbers: FONDECYT 1171406, PIA-ANILLO ACT172097, FONDECYT 1120201; Chilean National Fund for Scientific and Technological Development

Abstract

Obesity is a public health problem worldwide, and especially in women in reproductive age where more than one in three have obesity. Maternal obesity is associated with an increased maternal, placental, and newborn oxidative stress, which has been proposed as a central factor in vascular dysfunction in large-for-gestational-age (LGA) newborn. However, cellular and molecular mechanisms behind this effect have not been elucidated. Untreated human umbilical artery endothelial cells (HUAEC) from LGA (LGA-HUAEC) presented higher O_2^- levels, superoxide dismutase activity and heme oxygenase 1 messenger RNA (mRNA) levels, paralleled by reduced GSH:GSSG ratio and *NRF2* mRNA levels. In response to an oxidative challenge (hydrogen peroxide), only HUAEC from LGA exhibited an enhanced Glutathione Peroxidase 1 (*GPX1*) expression, as well as a more efficient antioxidant machinery measured by the biosensor probe, HyPer. An open state of chromatin in the TSS region of *GPX1* in LGA-HUAEC was evidenced by the DNase-HS assay. Altogether, our data indicate that LGA-HUAEC have an altered cellular and molecular antioxidant system. We propose that a chronic pro-oxidant intrauterine milieu, as evidenced in pregestational obesity, could induce a more efficient antioxidant system in fetal vascular cells, which could be maintained by epigenetic mechanism during postnatal life.

KEYWORDS
endothelial cells, epigenetics, large-for-gestational-age (LGA), maternal obesity, oxidative stress

[Correction added on 08 Apr 2019, after first online publication: the grant number is corrected]

1 | INTRODUCTION

Pregestational obesity and excessive weight gain during pregnancy are associated with high blood pressure, altered lipid profile, insulin resistance, and obesity in the offspring (Adamo, Ferraro, & Brett, 2012; Oken & Gillman, 2003). The cellular and molecular mechanisms underlying the alterations, caused by these maternal conditions, are not completely understood. Oxidative stress is one of the causes of obesity-related diseases (Marseglia et al., 2015), and elevated systemic markers of oxidative stress are reported in women with pregestational obesity and in the umbilical cord blood from large-for-gestational-age (LGA) newborn from mothers with obesity (LGA-MO; Malti et al., 2014)

Oxidative stress response involves the activation of the nuclear factor erythroid 2-related factor 2 (NFE2L2), whose gene product, NRF2, is a master transcription factor transactivating a plethora of antioxidant- and antixenobiotic protein-coding genes (Ma, 2013). NRF2 transactivates the antioxidant enzymes Glutathione Peroxidase 1 (GPX1), Heme Oxygenase 1 (HMOX1), and hydrogen peroxide (H_2O_2)-generating enzymes, such as NADPH oxidase 4 (NOX4) and superoxide dismutases (SODs; Ma, 2013). The genes coding for these pro- and antioxidant proteins are expressed in the human placenta and umbilical cord vascular cells (Barber, Robson, Myatt, Bulmer, & Lyall, 2001; Schneider et al., 2015). However, the possible alteration in the expression of these genes, in umbilical artery endothelium of LGA newborn, has not been described so far.

Epigenetic mechanisms explain how diverse phenotypes are mitotically inherited without a change in DNA sequence and how cell differentiation occurs from a single cell during development (Bird, 2007). DNA methylation by methyltransferases in mammalian cells (Reik, 2007) associates with gene repression and is inherited through cell division (Klose & Bird, 2006). Compaction and relaxation of chromatin structure require the presence and activity of ATP-dependent chromatin remodeling complexes allowing access to specific histones or DNA regions by altering the nucleosome positions (Kim, Samaranayake, & Pradhan, 2009). If chromatin structure is involved in the permanent effects that intrauterine redox-related adaptations in oxidative stress genes in LGA-derived endothelium has not been answered hitherto.

To answer these questions, we evaluated whether umbilical artery endothelial cells from LGA offspring from women with pregestational obesity show changes in their homeostatic redox capacity including the study of some of the most relevant genes and proteins expression as well as in vitro function.

2 | MATERIALS AND METHODS

2.1 | Samples

This research was conducted in accordance with the Declaration of Helsinki and Ethics Committee approval from the Faculty of Medicine at the Pontificia Universidad Católica de Chile. Patient informed consent was obtained at the moment of the maternity ward admission. Placentae were collected immediately after delivery from full-term offspring from normotensive, nonsmoking, non-alcohol, or drug consuming mothers, without any known medical or obstetrical complication. Maternal nutritional status, normal weight or obesity, was estimated calculating maternal BMI, corrected by gestational age (Rosso, 1985). Using a national standard curve (Milad et al., 2010) newborn were classified in accordance with the adequacy of weight for gestational age at birth. Neonates, between percentile 10th and 90th, were considered adequate for gestational age and over percentile 90th as LGA. Table 1 shows the maternal and neonatal general and anthropometric characteristics.

2.2 | Cell isolation and culture

Human umbilical artery endothelial cells (HUAEC) were isolated as previously described (Krause et al., 2013). Briefly, endothelial cells were isolated from umbilical arteries by collagenase digestion (0.2 mg/ml) and cultured (37°C, 5% CO_2) up to passage 3 in medium-131 containing microvascular growth supplement (MVGS), 3.2 mmol/l L-glutamine and 100 U/ml penicillin-streptomycin. All the experiments were made at passage 3 of the primary cell cultures. Before protein or messenger RNA (mRNA) extraction, confluent cells were starved by reducing the MVGS supplement to 2% and then exposed overnight to 7% O_2 (oxygen partial pressure ~33.9 mmHg, normoxia for this cell type) using a gas mixture (5% CO_2-balanced N_2) in a hypoxia chamber connected to a PROOX 110 device (BioSpherix, NY). On the next day, the cells were exposed (or not) to H_2O_2 (100 μM) for 3 hr.

2.3 | HUAEC infection with HyPer probe

Primary cultures of HUAEC, grown on 25 mm coverslips (5,000 cells/coverslip), were infected with 1:500 adenoviral dilution of HyPer. Two days after, the cells were ready for HyPer imaging as previously published (Román et al., 2017). The HyPer probe was constructed as follows. Briefly, cDNAs of cyto-HyPer (Evrogen, Moscow, Russia)

TABLE 1 Baseline characteristics of the study population.

	Control $n = 20$	LGA $n = 21$
Maternal variables		
Pregestational weight (g)	70.5 ± 1.20	88.2 ± 2.39****
Maternal height (m)	1.6 ± 0.01	1.6 ± 0.02
Maternal BMI	27.7 ± 0.18	34.0 ± 0.91****
Neonatal variables		
Gestational age (weeks)	38.5 ± 0.53	38.6 ± 0.19
Birth weight (g)	3464 ± 75.44	4168 ± 39.31****
Birth height (cm)	50.8 ± 0.60	52.2 ± 0.23**
Ponderal index	2.7 ± 0.07	2.9 ± 0.04**
Gender F/M	8/12	8/13

Ponderal index is expressed as birth weight × 100 × height^{-3} (g × cm^{-3}), and maternal body mass index (BMI) expressed as weight (kg) × height (m)$^{-2}$. F and M indicate a total number of female or male neonates. Values are mean ± S.E.M. or frequency.

Note. LGA: large-for-gestational-age.

***$p < 0.001$.

****$p < 0.0001$ determined by Mann–Whitney test or Chi^2, accordingly.

were sub-cloned into the commercial adenoviral vector pAdEasy-RFP with conventional molecular biology techniques, and homologous recombination was done by BJ5183 cells transformation. Recombinant adenoviral plasmids were digested with *Pac*I and transfected in HEK-AD 293 (AdHek) cells with lipofectamine according to the manufacturer's guidelines. Following the observation of the cytopathic effects (CPE), usually after 14–21 days, the cells were harvested and subjected to three freeze-thaw cycles, followed by centrifugation to remove cellular debris, and the resulting supernatant (2 ml) used to infect a 10 cm dish of 90% confluent AdHek cells. After the observation of CPEs, normally after 2–3 days, viral particles were purified and expanded by infecting 10 plates of AdHek cells (Hernández et al., 2018).

2.4 | Microscopy and imaging of HyPer biosensor

On the experimental day, the HUAEC medium was replaced by Krebs-Ringer-HEPES-glucose-glutamine (KRH) buffer (in mM: 140 NaCl, 4.7 KCl, 20 Hepes, 1.25 MgSO4, 1.25 CaCl2, pH 7.4) supplemented with 5 mM glucose and each coverslip was mounted in an open recording chamber. Images of HUAEC were registered using a Nikon Ti inverted microscope equipped with 40× oil objective [numerical aperture, N.A. 1.3]. A Xenon lamp was coupled to the monochromator device (Cairn Research Ltd, Faversham, UK). Digital images were acquired by means of a cooled CCD camera (Hamamatsu ORCA 03, Japan). All devices were synchronized and operated by using freeware micromanager software (Edelstein et al., 2014).

The HyPer biosensor is composed of a circular permuted yellow fluorescent domain, suitable for dual excitation at 420 and 490 nm. Emitted light from these two excitation channels was collected with a long-pass filter over 520 nm. The biosensor signals from both excitation wavelengths were acquired every 20 s and converted in a ratio (490/420) making H_2O_2 measurements reliable and independent of the biosensor expression in the cells.

The biosensor responses were measured in HyPer-expressing C-HUAEC and LGA-HUAEC taking into consideration a baseline of at least 10 min to ensure a stable recording. Then, H_2O_2 pulses were applied (1, 5, 10, 25, 50, 100, 200 μM) to build a dose-response curve. All HyPer recordings ended with 1,000 μM H_2O_2 pulse to obtain the maximal signal of the biosensor. With this experimental approach, measurements at equilibrium (baseline and peak values) along with kinetic analysis (rising and recovery signals) of biosensor were possible.

2.5 | Dihydroethidium assay

In a black wall 96-well plate, previously coated with 1% of gelatin, 3×10^4 C-HUAEC or LGA-HUAEC were seeded per well and incubated for 24 hrs. Before the Dihydroethidium (DHE) load, confluent cells were starved reducing to 2% the MVGS supplement and exposed overnight to 7% O_2. The cells were loaded with DHE (10 μM) and incubated for 30 min at 37°C in darkness. The cells were washed two times with 1× phosphate Buffered Saline (PBS; in mmol/l: 136 NaCl, 2.7 KCl, 7.8 Na2HPO4, 1.5 KH2PO4, pH 7.4), loaded with 4′,6-diamidino-2-phenylindole (DAPI; 300 nM) and incubated during 5 min at room temperature in darkness. The cells were washed two times with 1× PBS and maintained in KRH buffer (in mM: 140 NaCl, 4.7 KCl, 20 Hepes, 1.25 $MgSO_4$, 1.25 $CaCl_2$, pH 7.4) supplemented with 5 mM glucose. The fluorescence was measured immediately on a Synergy II microplate fluorescence reader (BioTek Instruments, VT), equipped with Gen5 software at excitation/emission wavelength 489/ < 580 nm and 358/461 nm, for DHE and DAPI, respectively. DHE fluorescence was normalized by DAPI fluorescence and presented as DHE/DAPI ratio.

2.6 | GSH:GSSG assay

Endothelial cells were grown in 60 mm culture dishes until they reached 70–80% confluence. Later, they were washed twice with PBS and scrapped in presence of hypotonic buffer (in M: NaCl 0.15, Na_2HPO_4 0.01, NaH_2PO_4 0.01, pH 7.4). The cell suspension was transferred to a 1.5 ml microtube and centrifuged at 1000*g* for 5 min at 4°C. After the supernatant was discarded, the pellet was resuspended in 1 ml of cold PBS. To ensure complete cell lysis, the cell homogenates were sonicated. The cell lysate (100 μl treated with 2 μl 2-vinylpyridine) were incubated at 37°C with 700 μl of potassium phosphate buffer with ethylenediaminetetraacetic acid (EDTA; KPE; 0.1 M potassium phosphate buffer with 5 mM EDTA disodium salt, pH 7.5), 60 μl of 280 μM NADPH and 60 μl 10 mM 5,5′-dithio-bis (2-nitrobenzoic acid) (DTNB) for 10 min at 30°C to oxidize all the GSH to GSSG. GSSG was then reduced by adding 60 μl GSH reductase. The rate of TNB formation was followed at 412 nm and was proportional to the sum of GSH and GSSG present. The rate was compared with a standard curve of GSH in the buffer.

2.7 | Determination of superoxide dismutase activity

This analysis was performed as described by Fridovich (Fridovich, 1995). In an aliquot of cell lysate (as previously described), the reduction of cytochrome by the superoxide radical in the xanthine/xanthine oxidase system was measured by spectrophotometry. Solution A was composed of 0.5 mM xanthine and 20 μM cytochrome c dissolved in PBS pH 7.8; Solution B contained xanthine oxidase and EDTA 0.1 mM (1:40). Enzymatic activity was detected at 550 nm after mixing 2.9 ml solution A, 50 μl solution B and 100 μl of sample, and expressed as units of enzyme/mg protein using the total protein determined with the Lowry method (Lowry, Rosebrogh, Farr, & Randall, 1951), using bovine serum albumin (BSA) as standard.

2.8 | Western blotting

Proteins from C-HUAEC or LGA-HUAEC (40 μg) were separated in polyacrylamide gel (12%) electrophoresis, including a lane with 7 μl of a prestained protein ladder (cat # 26619, Thermo Fisher Scientific), and transferred to 0.45 mm Polyvinylidene fluoride membranes (BioRad). Membranes were blocked with 5% BSA in Tris-buffered saline (TBS)

with 0.1% Tween (TBST) for 1 hr. The membranes were probed with anti-NRF2 antibody (Thermo Fisher Scientific Cat# PA5–27882, RRID:AB_2545358), rabbit monoclonal anti-NOX4 antibody (Abcam Cat# ab109225, RRID:AB_10861375), mouse monoclonal anti-β-Actin antibody (Sigma-Aldrich Cat# A5316, RRID:AB_476743), mouse monoclonal anti-HMOX1 antibody (BD Biosciences Cat# 610712, RRID:AB_398035), rabbit monoclonal GPX1 antibody (Abcam Cat# ab108427, RRID:AB_10890636), or mouse monoclonal SOD1 antibody (Abcam Cat# ab20926, RRID:AB_445919) for 1 hr at room temperature. Membranes were washed in TBST and incubated (1 hr, 22°C) in TBST containing horseradish peroxidase-conjugated goat antirabbit or antimouse secondary antibodies. Proteins were detected by enhanced chemiluminescence and quantified by densitometry using ImageJ (https://imagej.net, RRID: SCR_003070) as described elsewhere.

2.9 | Immunohistochemistry

The immunohistochemistry analysis of protein expression in umbilical arteries was done as previously reported (Schneider et al., 2015). Briefly, umbilical cords were washed with cold PBS, dissected in one vertical segment of 1 cm thick at2 cm from of the umbilical cord insertion, fixed for 24 hr at 4°C with neutral buffered formaldehyde solution (4% in PBS) and embedded in paraffin. Deparaffinized and rehydrated histological sections of 4 mm were subjected to heat-induced antigen retrieval using 100 mmol/l citrate buffer (pH 6.0) in a microwave for 15 min at maximal power. Samples were treated with 3% H_2O_2 in PBS for 30 min to room temperature to quench endogenous peroxidase activity. After rinsing in PBS for 5 min, all slides were incubated with 1% BSA and normal horse serum for 15 min at room temperature, to block nonspecific sites. Sections were incubated overnight at 4°C with primary anti-SOD1 (1:1,000; Abcam Cat# ab20926, RRID:AB_445919), NOX4 (1:500; Abcam Cat# ab109225, RRID:AB_10861375) and GPX1 (1:500; Abcam Cat# ab108427, RRID:AB_10890636) antibodies. The secondary antibody was added and then avidin-biotin-peroxidase complex (Vectastain Elite ABC reagent RTU Vector, Burlingame, CA) was applied for 30 min at room temperature, and 3 min of the chromogen 3′3-diaminobenzidine (DAB; Sigma) was used. Slides were counter-stained with Harris hematoxylin and permanently mounted. Specificity of the staining was determined by incubation of sections in the absence of the primary antibody. Sections were examined under an IX81-Olympus microscope, and images were captured using a digital camera (Olympus DP-71) and software (Olympus DP-BSW). At least two slides of every sample were analyzed for each antibody probed in three samples from each group.

The analyzes of the images were made using the ImageJ software (https://imagej.net, RRID: SCR_003070). Following the protocol previously described (Fuhrich, Lessey, & Savaris, 2013), the images were corrected subtracting the background, region of interest (ROI) containing 6–7 endothelial cells were selected using the drawing tool. The H DAB deconvolution plugin was used to separate immunostaining color (i.e. brown) from hematoxylin color (i.e. blue). The intensity of immunostaining was measured into the previously generated ROIs and the reciprocal intensities were calculated before statistical analyses (Nguyen & Nguyen, 2013).

2.10 | Isolation of total RNA and reverse transcription

Total RNA was isolated using Trizol (Invitrogen) as described (Krause et al., 2016). RNA quality and integrity were ensured by gel visualization and spectrophotometric analysis (OD260/280) and quantified at 260 nm. Aliquots of 1 μg of total RNA were reversed transcribed using IMPROM II RT kit (Promega).

2.11 | Quantitative polymerase chain reaction

Polymerase chain reactions were performed as described (Krause et al., 2013), using oligonucleotide primers for human genes of interest (GOI) *NRF2*, *FOXO3A*, *HMOX1*, *GPX1*, *TXNDR*, *PRDX3*, *PRDX6*, *SOD1* , *SOD2*, *p66sch*, and *NOX4*. Three different mRNAs, *RPLP0*, *RPLP2*, and *ATP5F1*, were selected as reference genes for relative quantity (RQ) calculation, because they showed the lowest standard deviation of raw Cts in all the experimental groups (data not shown), as it was previously described (Mane, Heuer, Hillyer, Navarro, & Rabin, 2008; Table 2). The PCR efficiency for each primer was calculated using a curve of cDNA made by five-fold serial dilutions (from 1× to 1/625×). All the amplifications were done using a 1/10 dilution of cDNA. Quantification was carried out using the algorithm proposed by Pfaffl (Pfaffl, 2001). The final RQ for each gene of interest (GOI) mRNA was calculated considering the geometrical mean of the three different reference genes.

2.12 | DNase hypersensitivity assay

The DNase hypersensitivity assay was performed as described by Stewart, Reik, and Schütz (1991). Control- and LGA-HUAEC were cultured in six-well plates until confluence. After washing with PBS, partial DNA digestion was performed by adding 1 ml digestion buffer (in mM Tris-HCl 15 mM pH 7.5, KC1 60 mM, NaCl 15 mM, $MgCl_2$ 5 mM, EGTA 0.5 mM, sucrose 300 mM, β-mercaptoethanol 0.5 mM, and NP40 0.5%) containing 0 U (Control) or 6.25 U of RQ1 DNase (Promega). After incubation for 5 min at room temperature (22–25°C), the digestion buffer was aspirated and cells were lysed with 0.5 ml of 50 mM Tris-HCl pH 8.0, 20 mM EDTA, 1% SDS, Proteinase K (200 μg/ml; Thermo Fisher Scientific) and RNase A (20 μg/ml) (Affymetrix); and incubated for 1 hr at 37°C. DNA was extracted by Phenol-chloroform method (Green & Sambrook, 2017). Twenty-five nanograms of DNA per reaction were used to amplify the *NRF2* transcription start site (TSS), *HMOX1* TSS, and *GPX1* TSS (GOI), and *PAX7* TSS as reference gene (Primer details in Table 3). The quantification was carried out using the algorithm proposed by Pfaffl (Pfaffl, 2001).

2.13 | Statistical analysis

The HyPer experiments were done in 21 and 57 single different C-HUAEC and LGA-HUAEC, respectively, derived from three

TABLE 2 Primers sequences and amplification conditions for mRNA RT-qPCR

mRNA Target	Forward sequence 5¨---3¨	Reverse sequence 5¨--- 3¨	Annealing T°	Efficiency (%)
NRF2	caactactcccaggttgccc	agtgactgaaacgtagccga	58°	109,5
HMOX1	caaagtgcaagattctgcccc	caactgtcgccaccagaaag	58°	96
FOXO3A	acaaacggctcactctgtcc	ggatggagttcttccagccg	60°	105
GPX1	agtgcgaggtgaacggtgcg	ggggtcggtcataagcgcgg	58°	94
PRDX3	tgccattccttggggcatt	catgaggaactggtgctgaat	58°	102,9
PRDX6	ctcgggactttaccccagtg	tgatatccttgctccaggca	58°	92,2
TXNDR1	gcatttgcagcagagcgaaa	tgccctcctgataagcaagaa	58°	97
SOD1	ggtgtggccgatgtgtctat	cctttgcccaagtcatctgc	58°	90,6
SOD2	tggggttggcttggtttcaa	tagtaagcgtgctcccacac	58°	97,9
NOX4	tccagtccttccgttggtttgc	cctttgcccaagtcatctgc	58°	99,4
p66sch	gaacaaatcacacctctgggc	cattgaagaattcaggggtcca	60°	99,5
ATP5F1	gccctgacagattctcctatcg	caataccctggacctaggaag	58°	103
RPLP0	aatctccaggggcaccattg	gaacacctgctggatgacca	58°	93
RPLP2	gcgccaaggacatcaagaag	ccagcaggtacactggcaa	56°	96

Note. mRNA: messenger RNA; RT-qPCR: real-time polymerase chain reaction.

different subjects per group. Protein and mRNA assays were carried out in replicates using at least four independents primary HUAEC cultures obtained from different umbilical cords. For DNase accessibility assays cell cultures from three different subjects per group were performed. For the superoxide quantification (DHE), SODs activity, GSH, and GSSG (GSH:GSSG ratio) the HUAEC from five subjects of each group were used. Values are mean ± S.E.M. or median ± interquartile range as indicated in each figure. Comparisons between two treatments or conditions were performed by Mann–Whitney U or *t* test, accordingly. All the analyses were carried out with the statistical software GraphPad Prism v6.01 (https://www.graphpad.com, RRID: SCR_015807). A value of $p < 0.05$ was considered the cut-off for statistical significance.

3 | RESULTS

3.1 | LGA-HUAEC have an altered redox status and an increased exogenous H_2O_2 buffering capacity

To evaluate if LGA-HUAEC present a modified redox status, such as altered antioxidant machinery, we used HyPer, an oxidative stress biosensor, combined with H_2O_2 pulses. Control- or LGA-HUAEC were infected with adenoviral particles containing HyPer and left proliferate for 48 hr before H_2O_2 treatment. Figure 1, shows representative curves obtained in C-HUAEC (Figure 1a) and LGA-HUAEC (Figure 1b), respectively. Before any treatment, baseline ratio values were recorded until evident stability was reached. Steady-state HyPer values from LGA-HUAEC were consistently higher than those observed in C-HUAEC (Figure 1c), suggesting a higher oxidant tone in LGA-HUAEC, possibly because of higher levels of endogenous H_2O_2 or a diminished disulfide reducing activity.

To assess the antioxidant machinery in LGA-HUAEC the EC_{50} of hyper fluorescence was estimated by recording the biosensor responses to increasing exogenous H_2O_2 concentrations. These responses were later referred to a percentage of the value obtained to the maximal stressor tested (1 mM H_2O_2). The maximal value obtained for the cells from both groups was comparable, indicating that dynamic ranges of the biosensor were comparable between groups. The EC_{50} values were 44.9 μM and 104.9 μM for C-HUAEC and LGA-HUAEC, respectively (Figure 1d). The difference in the EC_{50} between groups indicates that LGA-HUAEC have an increased exogenous H_2O_2 buffering capacity compared to C-HUAEC. It is noteworthy to point that independent of the cell group tested, the biosensor responses were always transient upon removal of the oxidant pulse, indicating that an intrinsic property of the cytosolic environment acts on the biosensor redox status.

TABLE 3 Primers sequences and amplification conditions for gDNA qPCR

gDNA Target	Forward sequence 5¨--- 3¨	Reverse sequence 5¨--- 3¨	Annealing T°	Efficiency (%)
NRF2 TSS	ctggagttcggacgctttga	ttctcgggcggtaaagtgag	58	98
HMOX1 TSS	tggccagactttgtttccca	tgaggacgctcgagaggag	58	97
GPX1 TSS	ggacgcgtgctcctcctaag	cccacatcctaactcaggaacc	64	103
PAX7 TSS	taaaagaaaagtccgaacctatc	gtttcagggctggacgga	60	90

Note. gDNA: genomic DNA; qPCR: quantitative polymerase chain reaction.

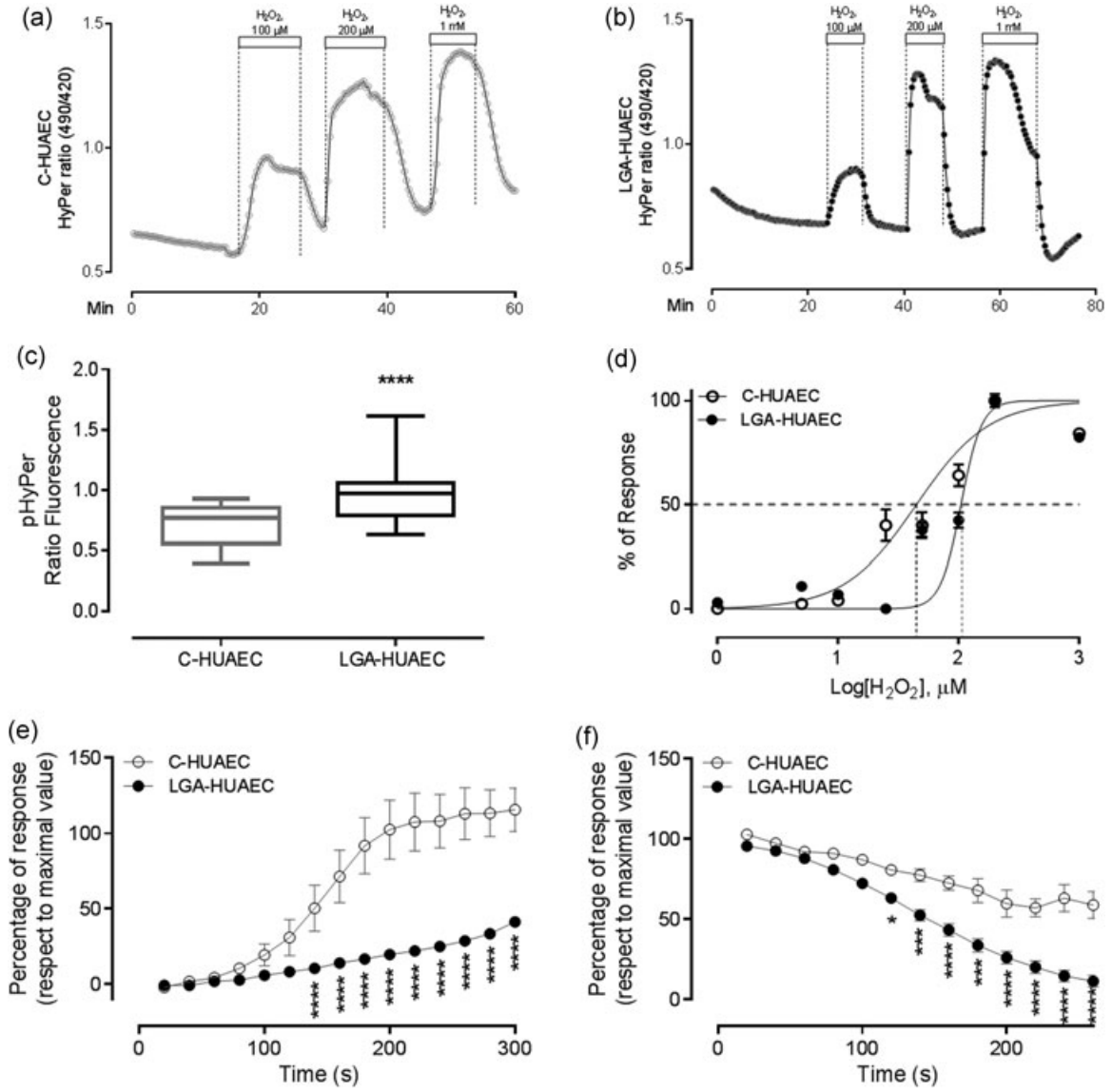

FIGURE 1 Indirect H_2O_2 measurement in C-HUAEC and LGA-HUAEC by HyPer under basal and oxidative stress conditions. (a) and (b) Representative data obtained by HyPer in control- and LGA-HUAEC, respectively. After transduction of HUAEC with HyPer, the cells were washed and placed with Krebs buffer to achieve resting conditions. Under an epifluorescence microscope, excitation was performed at 420 and 490 nm and fluorescence were acquired at 530 nm every 20 s for resting conditions and after a curve of H_2O_2 concentration 1–200 µM) for each experiment, ending with a 1,000 µM dose for calibration purposes. (c) Basal fluorescence of HyPer-probe in C- and LGA-HUAEC. Fluorescence at the end stabilizing stage were compared between C-HUAEC and LGA-HUAEC. In the box plots, the mean, the interquartile range are indicated. The end of whiskers indicate the minimal and maximal values, respectively. ****$p < 0.0001$, Mann–Whitney test. (d) The H_2O_2 concentration-response curve. The highest fluorescence reached with every H_2O_2 concentration were used to calculate and to compare EC50, in C- and LGA-HUAEC, in a normalized percentage of response vs log H_2O_2 concentration curve. EC50 were 44.89 and 104.9 µM for C-HUAEC and LGA-HUAEC, respectively. Values are mean ± S.E.M. (C-HUAEC $n = 3$, 21 replicates and LGA-HUAEC $n = 3$, 57 replicates). (e) HyPer signal increment following H_2O_2 challenge. A normalized percentage of response *vs* time (seconds) was made with fluorescence collected during the first 300 s of 100 µM H_2O_2 treatment. C-HUAEC data fitted in a nonlinear Boltzmann sigmoidal curve. Linear regression was used to calculate LGA-HUAEC fluorescence kinetic data. Values are Mean ± S.E.M. ****$p < 0.0001$, Two-way ANOVA, Bonferroni's multiple comparisons test. (C-HUAEC $n = 3$, 14 replicates and LGA-HUAEC $n = 3$, 49 replicates) (f) HyPer signal reduction following H_2O_2 withdraw. A normalized percentage of response vs time (seconds) was made with fluorescence collected during the first 260 s after H_2O_2 withdraw. Linear regression was used to calculate both C- and LGA-HUAEC fluorescence kinetic data. Values are Mean ± S.E.M. ***$p < 0.001$, two-way ANOVA, Bonferroni's multiple comparisons test (C-HUAEC $n = 3$, 21 replicates and LGA-HUAEC $n = 3$, 57 replicates). ANOVA: analysis of variance; H2O2: hydrogen peroxide; HUAEC: human umbilical artery endothelial cells; LGA: large-for-gestational-age

The kinetics of the biosensor was further analyzed to assess if the antioxidant performance of LGA-HUAEC differed from C-HUAEC. With this purpose in mind, the HyPer signal values obtained in the first 300 s after H_2O_2 treatment (100 μM) were used to compare the kinetics of increase in both groups (Figure 1e). The C-HUAEC curve reached an equilibrium between 200–300 s after the H_2O_2 pulse. On the other side, the HyPer signal from LGA-HUAEC showed a significant slower biosensor response (Figure 1e and Table 4). Several parameters related to HyPer fluorescence kinetic were calculated for each group. The slope, taken from the linear phase of the curve 80–180 s), was 0.83 ± 0.16/cent/s for C-HUAEC; and 0.14 ± 0.02/cent/s for LGA-HUAEC. The half-time value was calculated resulting in 144.9 ± 10 s for C-HUAEC and 196 ± 7.6 s for LGA-HUAEC. Finally, the area under the curve (AUC) of HyPer fluorescence in LGA-HUAEC was smaller than C-HUAEC AUC (Table 4). All these data indicate that LGA-HUAEC present a delayed and diminished oxidation of the HyPer probe by H_2O_2, suggesting that these cells have a constitutional efficient intracellular antioxidant machinery.

Hyper signal recovery results, which indicate the reduction of disulfide bond on the biosensor, suggests a higher reductive capacity of these cells. To check if LGA-HUAEC had an altered reductive system, we compared the decay of biosensor signal during the first 260 s after H_2O_2 withdrawal. Figure 1f and Table 4 show significant differences between the fluorescence level reached by C- and LGA-HUAEC in the recovery curves. The slope of the decreasing curve 80–180 s) was − 0.23 ± 0.05 and − 0.48 ± 0.04 for C-HUAEC and LGA-HUAEC, respectively. The fluorescence decay half-time was calculated in 123.4 ± 11.9 s for C-HUAEC whereas for LGA was 140 ± 4.1 s. On the other hand, the AUC analysis confirms that the recovery of the biosensor signal was significantly lower in LGA-HUAEC compared with control (Table 4). These results indicate a higher and faster rate of recovery of the probe, and therefore a higher capacity to reduce H_2O_2-oxidized cysteine residues in LGA-HUAEC.

The results obtained with this tool, that allows the monitoring of the peroxide neutralizing system and disulfide reducing activity in vivo, indicating that LGA-HUAEC seem to have a more robust antioxidant/reductive system compared with control cells.

TABLE 4 Parameters of HyPer fluorescence kinetics in C-HUAEC and LGA-HUAEC.

		C-HUAEC	LGA-HUAEC
Increment	Maximum reached (%)	115.7 ± 53.5	41.29 ± 23.4****
	Slope (percent/s)	0.83 ± 0.16	0.14 ± 0.02****
	Half-time (s)	144.9 ± 10	196 ± 7.6****
	AUC	18089 ± 11749	4480 ± 2683***
Recovery	Minimum reached (%)	58.94 ± 38.2	11.42 ± 27.1****
	Slope (percent/s)	−0.23 ± 0.05	−0.48 ± 0.04****
	Half-time (s)	123.4 ± 11.9	140 ± 4.1****
	AUC	18644 ± 3619	13441 ± 3969****

Maximum and minimum reached are the last data collected in increment and recovery curves, respectively. The slope of each curve was calculated between 80 and 180 s, which matches a clear increase and reduction of fluorescence in the increment and recovery curves, respectively. AUC = Area under the curve. Values are mean ± SEM.

Note. AUC: area under the curve; HUAEC: human umbilical artery endothelial cells.

***p < 0,001.

****p < 0,0001 determined by t test with Welch's correction (C-HUAEC n = 3, 21 experimental replicates and LGA-HUAEC n = 3, 57 experimental replicates).

3.2 | LGA-HUAEC have reduced superoxide anion level and increased SOD activity

To evaluate if increased basal level of H_2O_2 in LGA-HUAEC could be because of an increase in the SOD activity, the levels of superoxide anion, using the DHE fluorescent probe and the SOD activity were measured in C- and LGA-HUAEC. Figure 2a shows that LGA-HUAEC present a significant reduction of DHE and an increased SOD activity (Figure 2b).

3.3 | LGA-HUAEC have reduced GSH:GSSG ratio

Because increased levels of H_2O_2 in LGA-HUAEC suggest an intracellular pro-oxidant environment, the levels of reduced (GHS) and oxidized (GSSG) glutathione were measured, and the GHS:GSSG ratio calculated. As shown in Figure 2c, the GSH:GSSG ratio is reduced in LGA-HUAEC, associated to a diminished level of GSH (Figure 2d), without changes in the GSSG levels (Figure 2d), when compared with C-HUAEC.

3.4 | LGA-HUAEC do not present changes in pro- or antioxidant proteins expression

We later quantified pro- and antioxidant protein levels in C- and LGA-HUAEC to verify if the results obtained with the HyPer probe could be explained with changes in the expression of some of the proteins involved in the intracellular oxidative status. Figures 3a and b show representative Western blots of NRF2, NOX4, HMOX1, GPX1, and SOD1, respectively, using β-actin as an internal control. Although, NOX4 (Figure 3c) and GPX1 (Figure 3g) protein levels are elevated in LGA-HUAEC, the difference with C-HUAEC did not reach statistical significance, as well as HMOX1 (Figure 3d), NRF2 (Figure 3e), and SOD1 (Figure 3f). These data suggest that the protein levels in the HUAEC homogenates do not explain the functional results revealed by HyPer.

3.5 | Umbilical arteries endothelium from LGA newborn form women with pregestational obesity (LGA-OM) show altered levels of pro- and antioxidant enzymes

To evaluate the in situ levels of pro- and antioxidant enzymes, histological sections from umbilical cords from Control and LGA-OM were immunoassayed for NOX4, GPX1, and SOD1 enzymes (Figure 4a). As shown in Figure 4b, the reciprocal intensity of NOX4 and SOD1 are increased in LGA-HUAEC; however, the GPX1 did not show any difference between the groups.

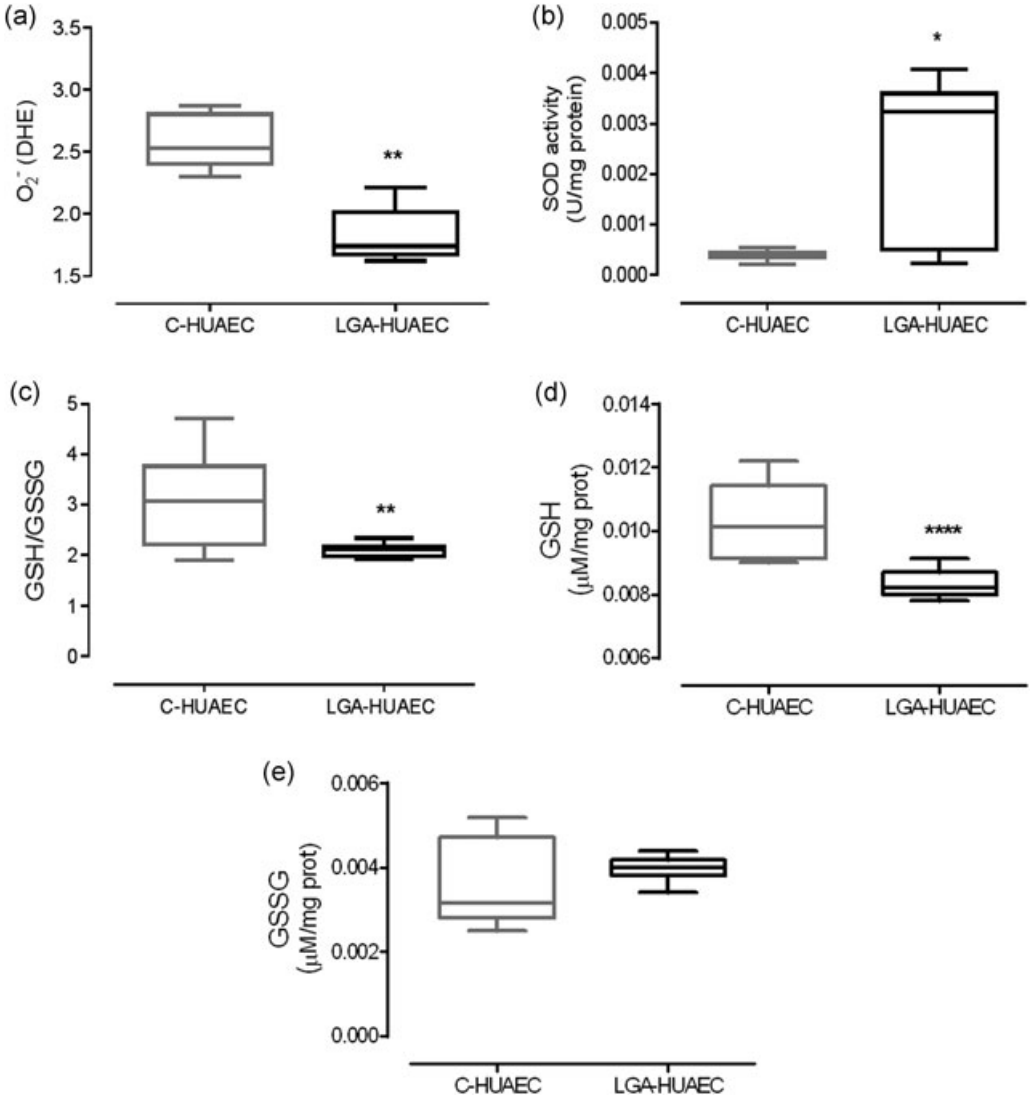

FIGURE 2 Basal superoxide anion level, SODs activity and quantitative measurement of GSH and GSSG in C-HUAEC and LGA-HUAEC. (a) Superoxide anion determination. C- and LGA-HUAEC were incubated with DHE 10 mM for 30 min at 37°C in darkness, washed three times with PBS previous incubation with DAPI 300 nM for 5 min in darkness at room temperature. Excesses of fluorescent molecules were rinsed three times. The cells were maintained Krebs buffer in darkness and immediately measured in a plate reader. DHE and DAPI fluorescence were acquired at (excitation/emission) 490/580 nm and 358/461 nm, respectively. $^{**}p < 0.01$, Mann–Whitney test, (C-HUAEC $n = 5$, LGA-HUAEC $n = 5$). (b) For the SODs activity, C- and LGA-HUAEC lysate (50 µl) were used to determine the reduction of cytochrome c by the superoxide radical in the xanthine/xanthine oxidase system. The activity was measured by 2 min at 37°C in a spectrophotometer at 550 nm. $^{*}p < 0.05$, Mann–Whitney test (C-HUAEC $n = 5$, LGA-HUAEC $n = 5$). (c–e) For the GSH/GSH assay, the C- and LGA-HUAEC lysate (100 µl) were incubated to 37°C and mixed with of KPE buffer, NADPH and DTNB to oxidize all GSH to GSSG and produce the TNB chromophore. The rate of TNB formation was followed by 2 min at 412 nm. The rate was compared with a standard curve of GSH and GSSG in the buffer. $^{**}p < 0.01$, $^{****}p < 0.0001$, Mann–Whitney test. (C-HUAEC $n = 5$, LGA-HUAEC $n = 5$). In the box plots, the mean, the interquartile range are indicated. The end of whiskers below and above the box indicate the minimal and maximal values, respectively. $^{****}p < 0.0001$, Mann–Whitney test. DAPI: 4′,6-diamidino-2-phenylindole; DHE: dihydroethidium; DTNB: 5,5′-dithio-bis (2-nitrobenzoic acid); HUAEC: human umbilical artery endothelial cells; LGA: large-for-gestational-age; SOD: superoxide dismutase

3.6 | LGA-HUAEC have altered *NRF2* and *HMOX1* gene expression

To verify whether LGA-HUAEC's augmented reducing capacity could be because of an altered antioxidant machinery, including transcriptional activation of genes, we determined the expression of several genes involved in the intracellular redox homeostasis. Using qPCR we calculated the RQ of *NRF2*, *FOXO3A*, *HMOX1*, *GPX1*, *TXNDR*, *PRDX3*, *PRDX6*, *SOD1* , *SOD2*, *p66sch*, and *NOX4* mRNAs in both C- and LGA-HUAEC (Figures 5a–k). However, the transcripts that could explain the biosensor data such as *GPX1*, *TXNDR*, *PRDX3*, *PRDX6*, *SOD1* , *SOD2*, *p66sch*, and *NOX4* mRNAs showed no significant differences between groups. Conversely, a decrease in *NRF2* (Figure 5a) and an increase in *HMOX1* gene expression (Figure 5c), which is a target of Nrf2, was observed in LGA-HUAEC.

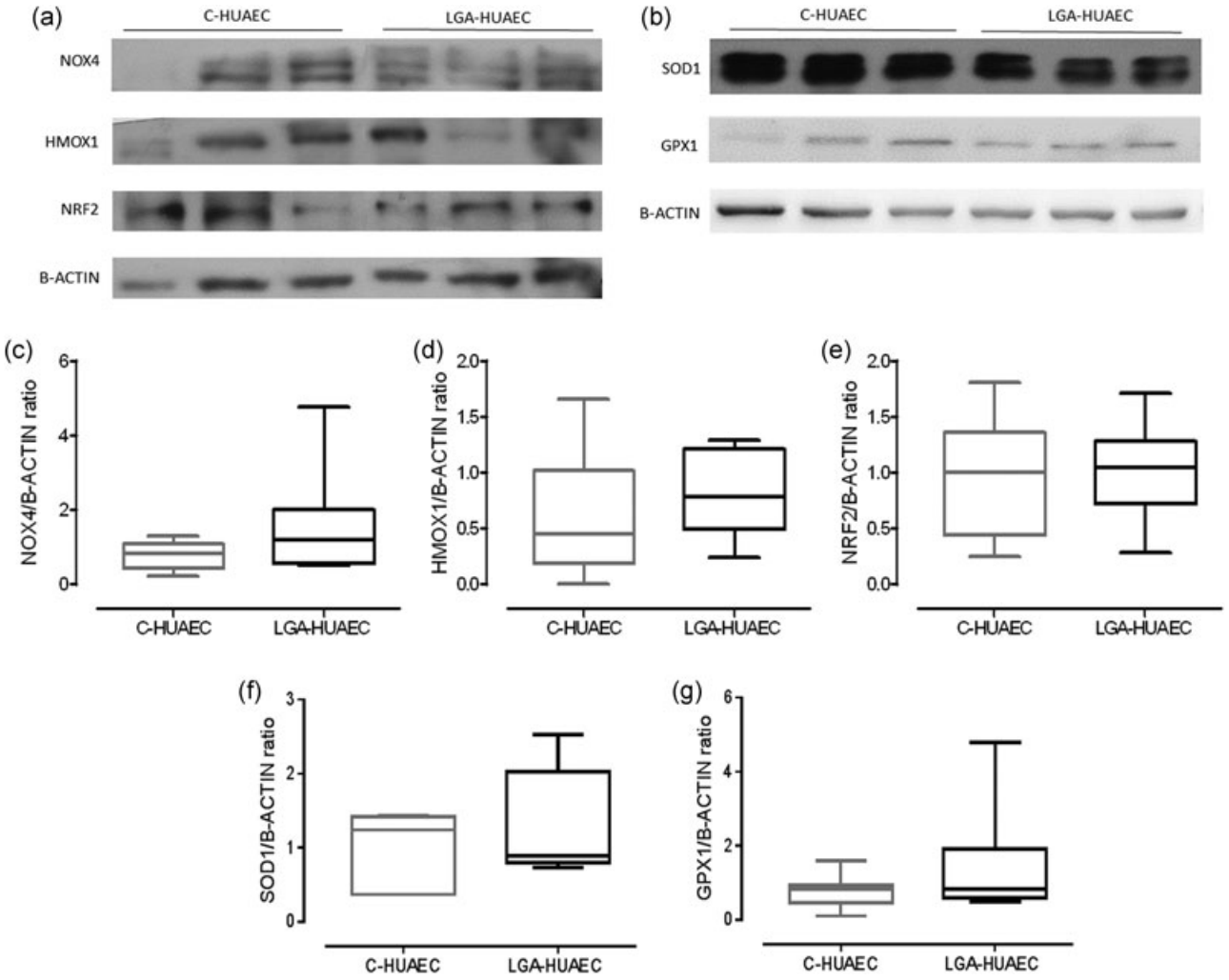

FIGURE 3 The basal protein level of antioxidant and pro-oxidant enzymes in C-HUAEC and LGA-HUAEC. (a) and (b) are representative Western blots for the proteins analyzed. The relative amount of NRF2 (c), HMOX1 (d), GPX1 (e), SOD1 (f), and NOX4 (g) between C- and LGA-HUAEC is presented. In the box plots, the mean, the interquartile range are indicated. The end of whiskers below and above the box indicate the minimal and maximal values, respectively. ****$p < 0.0001$, Mann–Whitney test (C-HUAEC $n = 8$, LGA-HUAEC $n = 11$). HUAEC: human umbilical artery endothelial cells; LGA: large-for-gestational-age; SOD: superoxide dismutase

3.7 | LGA-HUAEC overexpress the *GPX1* gene when exposed to a pro-oxidant stimulus

Following one of the premises of the "Developmental origins of health and disease (DOHaD)", where it has been proposed that the intrauterine oxidative stress milieu can reprogram the development and function of the offspring's cardiovascular system, we decided to evaluate the response of LGA-derived HUAEC to an oxidative challenge. To test this, HUAEC where exposed to a moderate oxidative challenge (100 μM H_2O_2, 3 hr) after which gene expression was evaluated. We detected a tenfold increase in *GPX1* mRNA levels in LGA-HUAEC, with no difference in C-HUAEC. Other transcripts, such as *NRF2*, *PRDX3*, and *SOD1*, showed no differences between groups (Figure 6a). This result suggests that LGA-HUAEC could have some early programming of oxidative stress response during intrauterine life.

3.8 | *GPX1* gene TSS has an open state of chromatin in LGA-HUAEC

To evaluate if epigenetic mechanisms could be implicated in the increased gene expression of *GPX1* in H_2O_2-challenged LGA-HUAEC compared with C-HUAEC, we assessed the chromatin state of *GPX1*, *NRF2*, *HMOX1*, *PRDX3*, and *SOD1* TSS. The magnitude of DNA digestion by DNase I depends directly on the chromatin state of the region evaluated. If chromatin has an open state (reduced nucleosome occupancy) DNase I can digest more DNA than in a closed state of the chromatin. In our approach, gDNA RQ after digestion was normalized by a constitutive closed chromatin region at *PAX7* TSS. Results show that there is no difference in the state of the chromatin at *NRF2*, *HMOX1*, *PRDX3* , and *SOD1* TSS between LGA- and C-HUAEC. However, there was higher DNA digestion in the *GPX1* TSS of LGA-HUAEC, indicating a more open state of chromatin in this proximal promoter site, compared with C-HUAEC (Figure 6b).

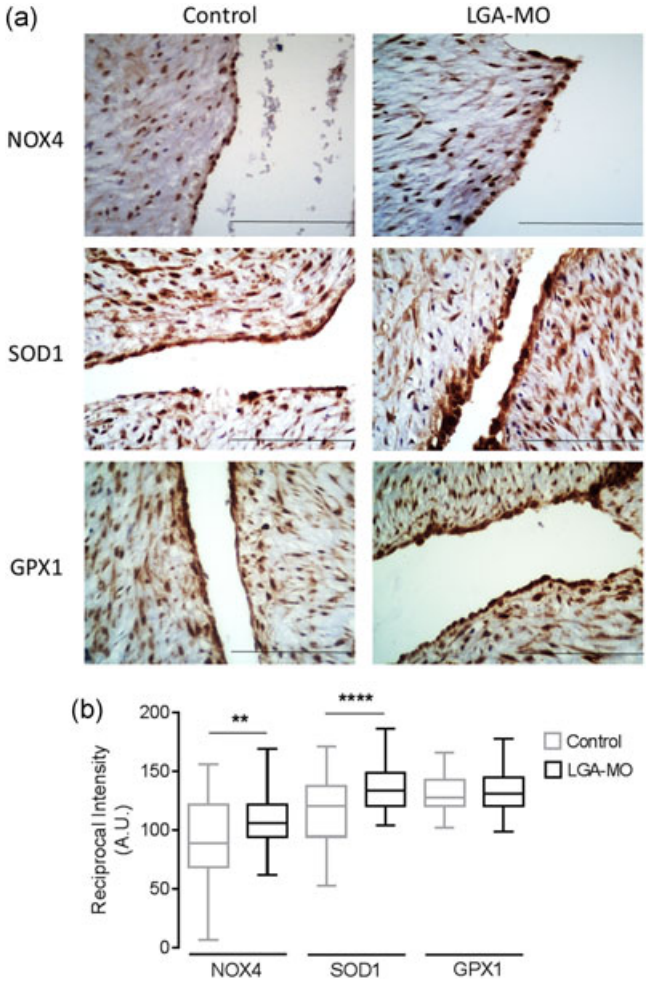

FIGURE 4 Umbilical artery endothelium in situ levels of H_2O_2 producing and reducing enzymes in Control and LGA-MO umbilical cords. (a) Representative microphotography from histological sections of umbilical cords stained for NOX4, SOD1, and GPX1. The intensity of DAB, in endothelial cells, was measured using HDAB color deconvolution plugin of Fiji version of the ImageJ software. Scale bar = 200 μm. (b) Statistical analyses of reciprocal intensity from NOX4, SOD1 and GPX1 in Control and LGA-MO umbilical cords. In the box plots, the mean, the interquartile range are indicated. The end of whiskers below and above the box indicate the minimal and maximal values, respectively. $^{**}p < 0.01$, $^{****}p < 0.0001$, Mann–Whitney test (C-HUAEC $n = 5$ and LGA-HUAEC $n = 5$), where 40 groups of six cells (C-HUAEC) and 57 groups of six cells (LGA-HUAEC) were analyzed. DAB: 3′3-diaminobenzidine; H_2O_2: hydrogen peroxide; HUAEC: human umbilical artery endothelial cells; LGA: large-for-gestational-age; SOD: superoxide dismutase [Color figure can be viewed at wileyonlinelibrary.com]

4 | DISCUSSION

Among chronic diseases, cardiovascular conditions have become one of the most common causes of death worldwide. It is now very clear that the intrauterine environment has a pivotal role in the risk of developing cardiovascular disease later in life. LGA newborn have an increased hazard risk of developing metabolic syndrome in their childhood (Boney, Verma, Tucker, & Vohr, 2005). LGA newborn from women with obesity present increased oxidative stress markers in the umbilical cord (Malti et al., 2014; Saker et al., 2008) associated with a decreased relaxation of chorionic arteries (Schneider et al., 2015). However, the cellular and molecular mechanisms by which this intrauterine environment can program the artery endothelial cell response to an oxidative challenge have not been clarified. The results shown in this work indicate that LGA-HUAEC presented a basal pro-oxidant status characterized by increased H_2O_2 levels and decreased GSH:GSSG ratio. The cells also have lower levels of superoxide anion associated to a high SOD activity and elevated SOD1 and NOX4 protein levels in LGA-derived umbilical artery endothelium. A pro-oxidant challenge (peroxide) unveiled an increased H_2O_2 buffering capacity and an elevated disulfide reducing activity in LGA-HUAEC together with altered gene expression of critical antioxidant enzymes and changes in chromatin structure in the promoter of *GPX1*, strongly suggesting the participation of epigenetic mechanisms (summarized in Figure 7).

Earlier evidence has pointed out to oxidative stress as a common feature in cardiovascular programming in LGA offspring (Malti et al., 2014; Schneider et al., 2015). However, to date, no report has shown the mechanisms involved in this adaptation in artery endothelial cells isolated from LGA newborn exposed to maternal pregestational obesity.

The H_2O_2-biosensor HyPer, which has been useful to characterize redox homeostatic changes in living cells (Kallens et al., 2017; Román et al., 2017), evidenced that LGA-HUAEC elicited an increased oxidative tone at steady-state. The later could be explained by the elevated SODs activity together with the higher in situ SOD1 protein expression, which is supported by the reduced level of superoxide anion observed in LGA-HUAEC. The increased expression of NOX4 in LGA-derived umbilical artery endothelium could be participating in the altered redox status in this condition (Martyn, Frederick, von Loehneysen, Dinauer, & Knaus, 2006). All these findings reflect the fine equilibrium between oxidative and reductive forces operating simultaneously in LGA-HUAEC.

Glutathione (GSH) is the major nonenzymatic cellular antioxidant (Dickinson & Forman, 2002). GPX uses GSH to reduce oxidized proteins generating the oxidized form of glutathione (GSSG; Brigelius-Flohé & Maiorino, 2013). The intracellular GSH:GSSG ratio is broadly used to evaluate cell redox status (Locigno & Castronovo, 2001; Noctor & Foyer, 1998). The observation in our model that LGA-HUAEC had a lower GSH:GSSG ratio, due to lower levels of GSH, support the proposal that these cells exhibit a pro-oxidant status, as suggested by the results with the HyPer probe.

The analysis of the kinetics of the HyPer probe signals is useful to visualize the intrinsic components of the antioxidant machinery could be participating in the LGA-induced redox adaptations. The rate of the rising signal observed in the biosensor after the exogenous H_2O_2 pulses reflect the combination of two cellular aspects: the H_2O_2 permeability at plasma membrane defined mainly by aquaporins (Bienert & Chaumont, 2014; Miller, Dickinson, & Chang, 2010) and the capacity of H_2O_2 to oxidize thiols on cytoplasmic proteins, since HyPer depends of peroxiredoxins (Stöcker, Maurer, Ruppert, & Dick, 2017).

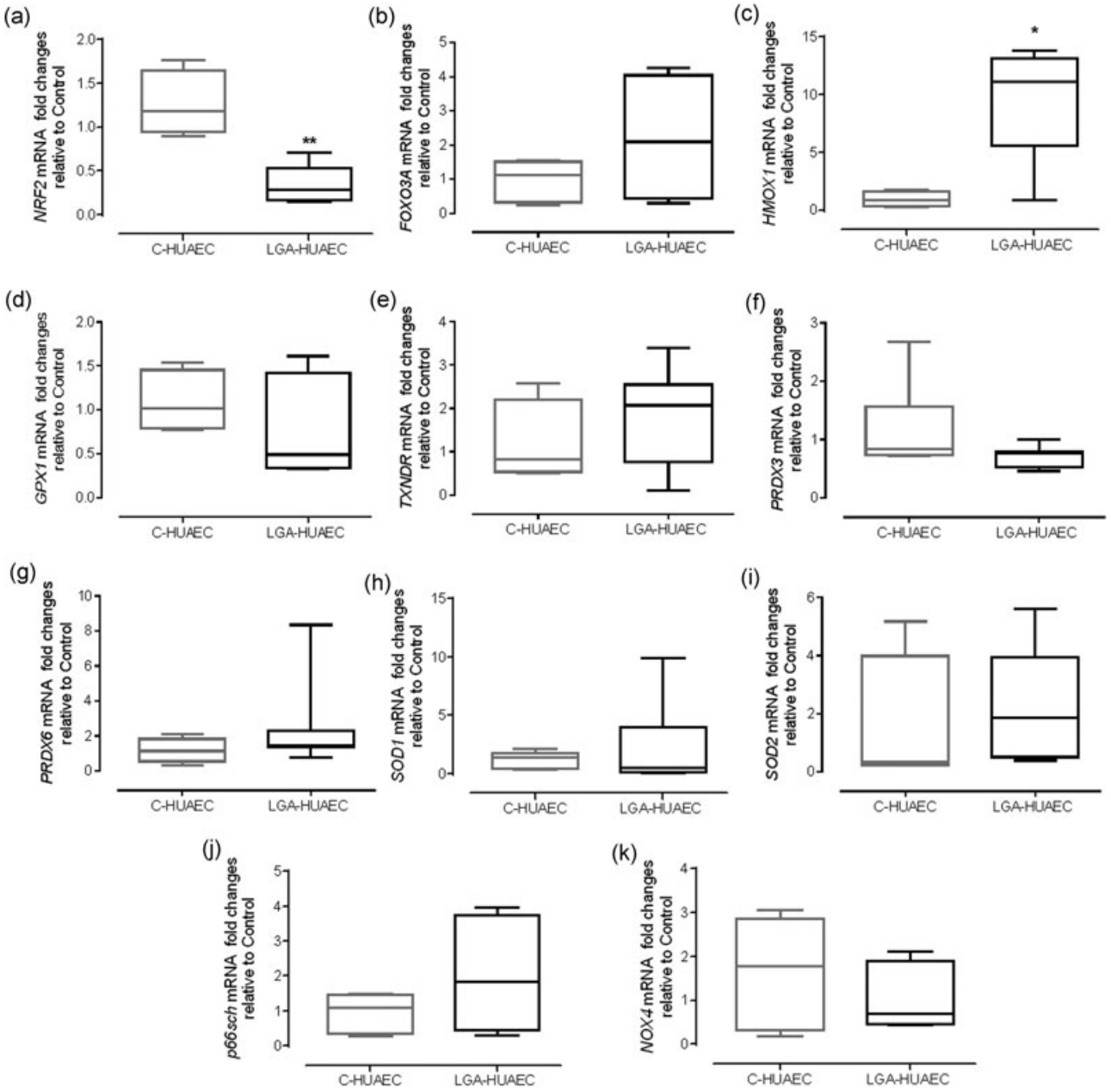

FIGURE 5 Basal mRNA level of genes involved in the antioxidant and pro-oxidant response in C-HUAEC and LGA-HUAEC. Total RNA was extracted with Trizol and quantified. The cDNA was obtained from 500 ng of RNA by reverse transcription. Relative quantities of mRNA for *NRF2* (a), *FOXO3A* (b), *HMOX1* (c), *GPX1* (d), *TXNDR* (e), *PRDX3* (f), *PRDX6* (g), *SOD1* (h), *SOD2* (i), *p66sch* (j) and *NOX4* (k) comparing between C-HUAEC and LGA-HUAEC was performed by qPCR. In the box plots, the mean, the interquartile range are indicated. The end of whiskers below and above the box indicate the minimal and maximal values, respectively. $^{*}p < 0.05$ $^{**}p < 0.01$, Mann–Whitney test (C-HUAEC $n = 4$, LGA-HUAEC $n = 7$). HUAEC: human umbilical artery endothelial cells; LGA: large-for-gestational-age; mRNA: mesenger RNA; qPCR: quantitative polymerase chain reaction

Our experiments indicate that after H_2O_2 exposure, LGA-HUAEC produce a slower increase in the biosensor signal compared to control cells, indicating that these cells better endure extracellular oxidant challenges. Moreover, LGA-HUAEC showed to be more efficient to recover the HyPer signal than control cells, likely due to better adapted machinery to reduce disulfide bonds on cytoplasmic proteins. Thus, we propose that a chronic pro-oxidant fetal environment could modify the antioxidant machinery performance in LGA-HUAEC.

Then, we decided to evaluate if there was an altered expression of antioxidant-related genes in LGA-HUAEC. Edlow, Hui, Wick, Fried, and Bianchi (2016) analyzed the cord blood transcriptome of the offspring from mothers with obesity, evidencing altered segregation of mRNAs related to inflammatory signaling, glucose/lipid metabolism, and ROS homeostasis, in comparison to the newborn from lean mothers (Edlow et al., 2016). In nonhuman primates, the mRNA of the reductive enzyme *Rdh12* was increased, among other candidate

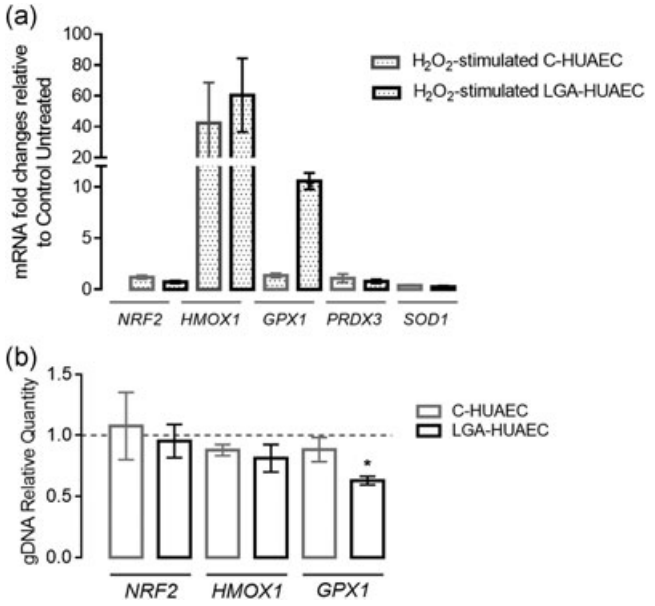

FIGURE 6 Transcript levels of antioxidant and pro-oxidant genes after H_2O_2 treatment and its chromatin accessibility in C-HUAEC and LGA-HUAEC. (a) Transcript levels of NRF2, HMOX1, GPX1, PRDX3, and SOD1 genes in C-HUAEC and LGA-HUAEC after H_2O_2 treatment. The cells were challenged with 100 μM of H_2O_2 for 3 hr. Then, total RNA was extracted with Trizol and quantified, 500 ng of RNA was reverse-transcribed, and qPCR was performed. Values are mean ± S.E.M. *$p < 0.05$ vs C-HUAEC, Man–-Whitney test (C-HUAEC $n = 3$, LGA-HUAEC $n = 3$). (b) The DNase hypersensitivity assay for antioxidant gene promoters. Primary C-HUAEC and LGA-HUAEC were lysed and the DNA obtained was digested with zero or 6,25 U of DNase I for 5 min at 22°C. The Genomic DNA (gDNA) was extracted by the phenol-chloroform method and quantified. Using 25 ng of gDNA, relative quantities of *NRF2*, *HMOX1*, and *GPX1* gDNA were calculated using *PAX7* as endogenous control. Values are mean ± S.E.M. *$p < 0.05$ vs C-HUAEC, Mann–Whitney test (C-HUAEC $n = 3$, LGA-HUAEC $n = 3$). H2O2: hydrogen peroxide; HUAEC: human umbilical artery endothelial cells; LGA: large-for-gestational-age

genes analyzed, in the liver of the offspring of dams fed a high-fat diet (Aagaard-Tillery et al., 2008). Under basal conditions, we found that LGA-HUAEC have downregulation of *NRF2* and an increase in *HMOX1* mRNA, both antioxidant proteins, indicating possible programming of gene expression associated to a chronic pro-oxidant milieu secondary to maternal obesity

The lack of induction of *NRF2* mRNA by oxidative stress could be explained by the fact that NRF2 actions depend mainly on its protein degradation/stabilization, and less on its gene transcription. It has been reported that NRF2 is constitutively degraded at the proteasome by Keap1-dependent ubiquitination (McMahon, Itoh, Yamamoto, & Hayes, 2003; Nguyen, Sherratt, Nioi, Yang, & Pickett, 2005). Oxidative stress induces the release of NRF2 from Keap-1, allowing its stabilization and nuclear translocation, where it binds to the gene promoter of target genes (Nguyen, Sherratt, Huang, Yang, & Pickett, 2003). This action of NRF2 does not depend on its transcription rate but mainly on its protein stability and nuclear translocation (Nguyen, Nioi, & Pickett, 2009). In the Western blot experiments performed, the whole cell homogenates were analyzed, and no difference in the NRF2 protein was observed in LGA-HUAEC, compared with C-HUAEC. This result does not allow to differentiate between cytosolic and nuclear NRF2 protein location, which would have been an interesting contribution to these data.

Remarkably, LGA-HUAEC showed overexpression of *GPX1* mRNA in response to H_2O_2 treatment, compared with control, resembling the Epigenetic Transcriptional Memory (ETM) described in immune cells exposed to inflammatory mediators (D´Urso & Brickner, 2016; Gialitakis, Arampatzi, Makatounakis, & Papamatheakis, 2010). The ETM has been defined as an inducible gene overexpression when the same gene has been previously exposed to the same stimuli (Gialitakis et al., 2010; Light et al., 2013). ETM is explained by a first stimulus inducing regulatory proteins recruitment and an open state of the chromatin at the TSS of inducible genes. The TSS of *GPX1* gene in LGA-HUAEC showed a higher DNase sensitivity, indicating an open state of the chromatin. This could be because of previous regulatory protein recruitment that induced an enhanced response to the H_2O_2 challenge. If we consider the previously reported pro-oxidant environment in LGA fetuses from women with pregestational obesity (Catalano & Shankar, 2017; Malti et al., 2014), it is reasonable to ponder that oxidative response genes in LGA-derived HUAEC have been chronically stimulated during pregnancy, causing an epigenetic effect that can be mitotically inherited to cellular progeny. This mechanism could underlie the maintenance of an elevated risk of fast-onset endothelial dysfunction by future stressors in these subjects during their postnatal life (Gaillard, 2015).

The findings described here suggest the participation of oxidative stress, particularly H_2O_2, in the NO-dependent endothelial dysfunction observed in placental arteries from LGA newborn (Schneider et al., 2015). After 10 min of H_2O_2 stimulation, a PI-3K/Akt-dependent endothelial Nitric Oxide Synthase (eNOS) activation is observed in bovine aortic endothelial cells (BAEC; Cai et al., 2003). However, BAEC treated for 24 hr with H_2O_2 showed reduced levels of tetrahydrobiopterin (BH_4), a limiting cofactor for the eNOS activity, and its reducing enzyme dihydrofolate reductase (Chalupsky & Cai, 2005), leading to eNOS uncoupling and shifting to a superoxide-producing enzyme (Förstermann & Münzel, 2006). Thus, we propose that the previously described pro-oxidant intrauterine environment in pregnancies with LGA from women with obesity (Malti et al., 2014), leads LGA-HUAEC to shift to an adapted oxidative status. By the other hand, in genetic and chemical-induced oxidative cell models, a reduction of the GSH:GSSG ratio has been associated to endothelial dysfunction (Espinosa-Díez et al., 2018); characterized by eNOS uncoupling induced by elevated eNOS S-glutathionylation (Crabtree, Brixey, Batchelor, Hale, & Channon, 2013; Espinosa-Díez et al., 2018) and BH_4 oxidation to BH_2 (Crabtree et al., 2013). Our group has previously shown evidence for eNOS inactivation in LGA-HUAEC (Muñoz-Muñoz, Krause, Uauy, & Casanello, 2018).

To survive, prokaryotic and eukaryotic cells have the ability to modifying their cellular physiology in response to a pro-oxidant environment (Crawford & Davies, 1994; Lushchak, 2010). In the non-dividing human retinal pigmented epithelial cell line, chronic

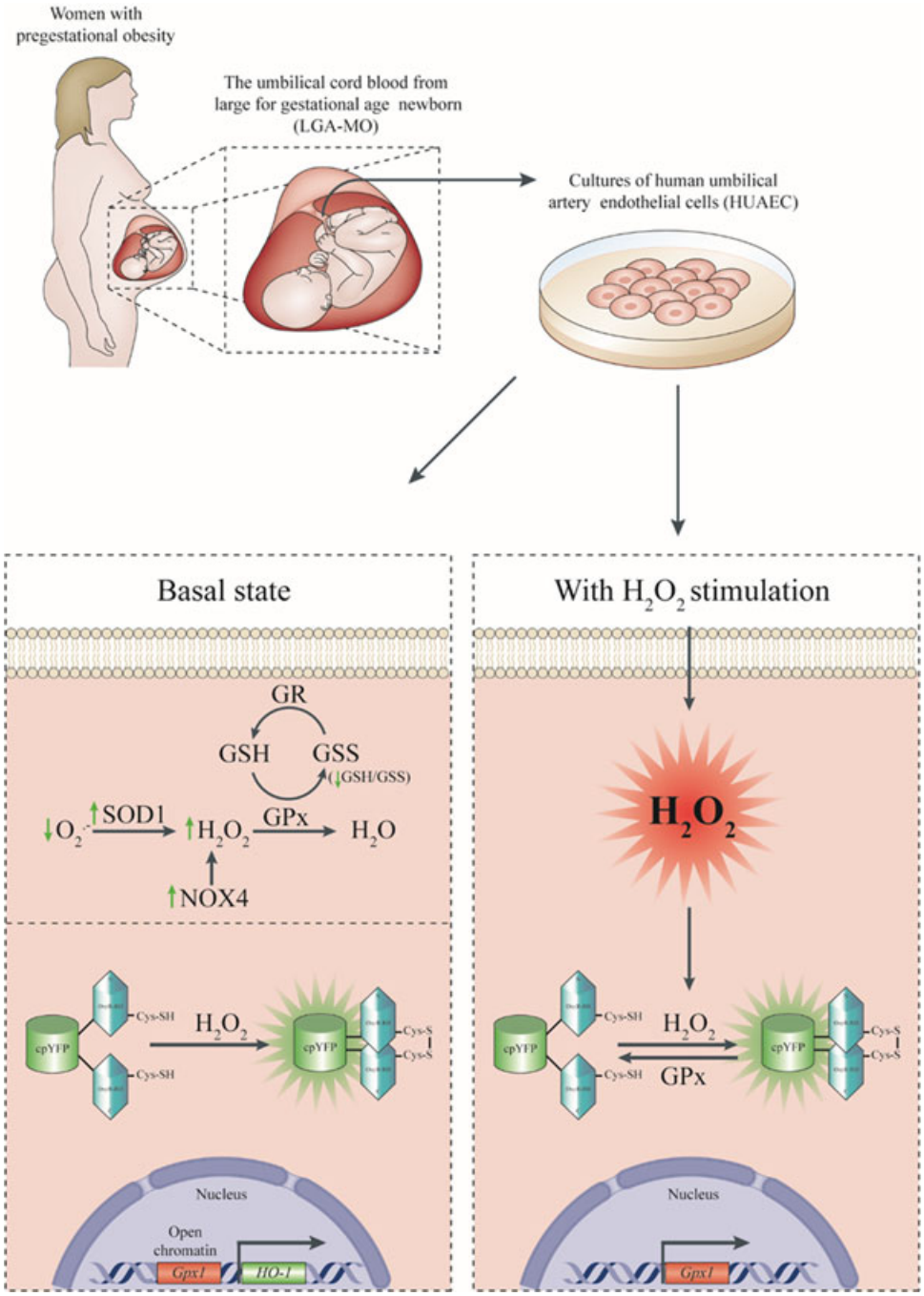

FIGURE 7 HUAEC from LGA-MO newborn shows a pro-oxidant status and a higher antioxidant performance. The altered redox status of LGA-HUAEC is characterized by increased H_2O_2 level and decreased GSH:GSSG ratio. The cells also showed a diminished level of superoxide anion associated with a high superoxide dismutase activity; associated with elevated protein levels of SOD1 and NOX4, both H_2O_2 producer enzymes. A pro-oxidant challenge revealed in LGA-HUAEC an increased H_2O_2 buffering capacity and an elevated reductive activity. In front of an oxidative stimulus, in LGA-HUAEC *GPX1* gene was overexpressed associated with an open chromatin structure at a basal level, strongly suggesting the participation of epigenetic mechanisms. H2O2: hydrogen peroxide; HUAEC: human umbilical artery endothelial cells; LGA: large-for-gestational-age [Color figure can be viewed at wileyonlinelibrary.com]

treatment with nonlethal H_2O_2 concentrations induced an increment of cell viability after lethal H_2O_2 treatment (3 mM, 1 hr). The later was achieved because of high levels of catalase, CuZn-SOD, and GPX1 activity (Jarrett & Boulton, 2005). A similar hormetic effect was found in mouse embryonic fibroblast cells subjected to repeated treatments with low concentrations of H_2O_2 (Pickering, Vojtovich, Tower, & A Davies, 2013). Hence, we propose that LGA-derived HUAEC, which are chronically exposed to a pro-oxidant intrauterine environment, exhibit an oxidative adaptation characterized by an increased superoxide neutralizing system, higher SOD activity, SOD1 and NOX4 induced protein expression, and an open chromatin status at the *GPX1* TSS.

Following the line of thought that support the early origins of chronic diseases (DOHaD), we propose that fetal endothelial cells from the offspring of women with pregestational obesity, exposed to oxidative stress during fetal development, can reprogram the redox system at a cellular and epigenetic level, to trigger a faster and more efficient response to subsequent oxidative-related insults.

5 | CONCLUSIONS

This work evidences for the first time an increased antioxidant machinery performance in HUAEC isolated from LGA newborn from women with pregestational obesity could impact the offspring's endothelial function at birth. On the basis of the findings in the gene expression and chromatin structure we propose that detrimental fetal environment could epigenetically modify the gene expression and thus function in endothelial vascular cells (Block & El-Osta, 2017; Mcmillen, 2005). The long-term effects of these cellular adaptations need to be further studied in the postnatal life of LGA offspring, to confirm that these early findings induced by an altered maternal and fetal nutritional environment during pregnancy could lead to a higher cardiovascular risk (Adamo et al., 2012; Oken & Gillman, 2003).

ACKNOWLEDGMENTS

This study was funded by the Chilean National Fund for Scientific and Technological Development, FONDECYT #1171406 and #1120201. We thank all the study participants for generously donating their samples for this research.

CONFLICT OF INTERESTS

The authors declare that there are no conflict of interests.

AUTHOR CONTRIBUTIONS

I.C.W, O.P, C.J, and P.C conceived and designed the experiments. I.C.W, O.P, C.H, and C.J collected and analyzed the experimental data. I.C.W, O.P, C.J, and P.C interpreted the experimental data. I.C.W, O.P, C.J, and P.C drafted the article that was approved by all authors.

ORCID

Paola Casanello http://orcid.org/0000-0002-2355-1476

REFERENCES

Aagaard-Tillery, K. M., Grove, K., Bishop, J., Ke, X., Fu, Q., McKnight, R., & Lane, R. H. (2008). Developmental origins of disease and determinants of chromatin structure: Maternal diet modifies the primate fetal epigenome. *Journal of Molecular Endocrinology*, *41*(1–2), 91–102. https://doi.org/10.1677/JME-08-0025

Adamo, K. B., Ferraro, Z. M., & Brett, K. E. (2012). Can we modify the intrauterine environment to halt the intergenerational cycle of obesity? *International Journal of Environmental Research and Public Health*, *9*(4), 1263–1307. https://doi.org/10.3390/ijerph9041263

Barber, A., Robson, S. C., Myatt, L., Bulmer, J. N., & Lyall, F. (2001). Heme oxygenase expression in human placenta and placental bed: Reduced expression of placenta endothelial HO-2 in preeclampsia and fetal growth restriction. *The FASEB Journal: Official Publication of the Federation of American Societies for Experimental Biology*, *15*(7), 1158–1168. https://doi.org/10.1096/fj.00-0376com

Bienert, G. P., & Chaumont, F. (2014). Aquaporin-facilitated transmembrane diffusion of hydrogen peroxide. *Biochimica et Biophysica Acta - General Subjects*. May. https://doi.org/10.1016/j.bbagen.2013.09.017

Bird, A. (2007). Perceptions of epigenetics. *Nature*, *447*(7143), 396–398. https://doi.org/10.1038/nature05913

Block, T., & El-Osta, A. (2017). Epigenetic programming, early life nutrition and the risk of metabolic disease. *Atherosclerosis*, *266*, 31–40. https://doi.org/10.1016/j.atherosclerosis.2017.09.003

Boney, C. M., Verma, A., Tucker, R., & Vohr, B. R. (2005). Metabolic syndrome in childhood: Association with birth weight, maternal obesity, and gestational diabetes mellitus. *Pediatrics*, *115*(3), e290–e296. https://doi.org/10.1542/peds.2004-1808

Brigelius-Flohé, R., & Maiorino, M. (2013). Glutathione peroxidases ☆. *BBA - General Subjects*, *1830*, 3289–3303. https://doi.org/10.1016/j.bbagen.2012.11.020

Cai, H. U. A., Li, Z., Davis, M. E., Kanner, W., Harrison, D. G., & Dudley, S. C. D. (2003). Akt-dependent phosphorylation of serine 1179 and mitogen-activated protein kinase kinase/extracellular signal-regulated kinase 1/2 cooperatively mediate activation of the endothelial nitric-oxide synthase by hydrogen peroxide. *Molecular Pharmacology*, *63*(2), 325–331.

Catalano, P. M., & Shankar, K. (2017). Obesity and pregnancy: Mechanisms of short term and long term adverse consequences for mother and child. *BMJ (Online)*, https://doi.org/10.1136/bmj.j1

Chalupsky, K., & Cai, H. (2005). Endothelial dihydrofolate reductase: Critical for nitric oxide bioavailability and role in angiotensin II uncoupling of endothelial nitric oxide synthase. *Proceedings of the National Academy of Sciences of the United States of America*, *102*(25), 9056–9061. https://doi.org/10.1073/pnas.0409594102

Crabtree, M. J., Brixey, R., Batchelor, H., Hale, A. B., & Channon, K. M. (2013). Integrated redox sensor and effector functions for tetrahydrobiopterin- and glutathionylation-dependent endothelial nitric-oxide synthase uncoupling. *Journal of Biological Chemistry*, *288*(1), 561–569. https://doi.org/10.1074/jbc.M112.415992

Crawford, D. R., & Davies, K. J. (1994). Adaptive response and oxidative stress. *Environmental Health Perspectives*, *102*(Suppl), 25–28. https://doi.org/10.1289/ehp.94102s1025

Dickinson, D. A., & Forman, H. J. (2002). Glutathione in defense and signaling: Lessons from a small thiol. *Annals of the New York Academy of Sciences*, *973*, 488–504.

D´Urso, A., & Brickner, J. H. (2016). Epigenetic transcriptional memory. *Current Genetics*, 1–5. https://doi.org/10.1007/s00294-016-0661-8

Edelstein, A. D., Tsuchida, M. A., Amodaj, N., Pinkard, H., Vale, R. D., & Stuurman, N. (2014). Advanced methods of microscope control using μManager software. *Journal of Biological Methods*, *1*(2), 10. https://doi.org/10.14440/jbm.2014.36

Edlow, A. G., Hui, L., Wick, H. C., Fried, I., & Bianchi, D. W. (2016). Assessing the fetal effects of maternal obesity via transcriptomic analysis of cord blood: A prospective case-control study. *BJOG: An International Journal of Obstetrics and Gynaecology*, *123*(2), 180–189. https://doi.org/10.1111/1471-0528.13795

Espinosa-Díez, C., Miguel, V., Vallejo, S., Sánchez, F. J., Sandoval, E., Blanco, E., & Lamas, S. (2018). Role of glutathione biosynthesis in endothelial dysfunction and fibrosis. *Redox Biology*, *14*(August 2017), 88–99. https://doi.org/10.1016/j.redox.2017.08.019

Fridovich, I. (1995). Superoxide radical and superoxide dismutases. *Annual Review of Biochemistry*, *64*(1), 97–112. https://doi.org/10.1146/annurev.bi.64.070195.000525

Fuhrich, D. G., Lessey, B. A., & Savaris, R. F. (2013). Comparison of HSCORE assessment of endometrial β3 integrin subunit expression with digital HSCORE using computerized image analysis (ImageJ). *Anal Quant Cytopathol Histpathol*, *35*(4), 210–216.

Förstermann, U., & Münzel, T. (2006). Endothelial nitric oxide synthase in vascular disease: From marvel to menace. *Circulation*, *113*(13), 1708–1714. https://doi.org/10.1161/CIRCULATIONAHA.105.602532

Gaillard, R. (2015). Maternal obesity during pregnancy and cardiovascular development and disease in the offspring. *European Journal of Epidemiology*, *30*(11), 1141–1152. https://doi.org/10.1007/s10654-015-0085-7

Gialitakis, M., Arampatzi, P., Makatounakis, T., & Papamatheakis, J. (2010). Gamma interferon-dependent transcriptional memory via relocalization of a gene locus to PML nuclear bodies. *Molecular and Cellular Biology*, *30*(8), 2046–2056. https://doi.org/10.1128/MCB.00906-09

Green, M. R., & Sambrook, J. (2017). Isolation of high-molecular-weight DNA using organic solvents. *Cold Spring Harbor Protocols*, *2017*(4), 356–359. https://doi.org/10.1101/pdb.prot093450

Hernández, H., Parra, A., Tobar, N., Molina, J., Kallens, V., Hidalgo, M., & Porras, O. (2018). Insights into the HyPer biosensor as molecular tool for monitoring cellular antioxidant capacity. *Redox Biology*, *16*, 199–208. https://doi.org/10.1016/j.redox.2018.02.023

Jarrett, S. G., & Boulton, M. E. (2005). Antioxidant up-regulation and increased nuclear DNA protection play key roles in adaptation to oxidative stress in epithelial cells. *Free Radical Biology and Medicine*, *38*(10), 1382–1391. https://doi.org/10.1016/j.freeradbiomed.2005.02.003

Kallens, V., Tobar, N., Molina, J., Bidegain, A., Smith, P. C., Porras, O., & Martínez, J. (2017). Glucose promotes a pro-oxidant and pro-inflammatory stromal microenvironment which favors motile properties in breast tumor cells. *Journal of Cellular Biochemistry*, *118*(5), 994–1002. https://doi.org/10.1002/jcb.25650

Kim, J. K., Samaranayake, M., & Pradhan, S. (2009). Epigenetic mechanisms in mammals. *Cellular and Molecular Life Sciences*, *66*(4), 596–612. https://doi.org/10.1007/s00018-008-8432-4

Klose, R. J., & Bird, A. P. (2006). Genomic DNA methylation: The mark and its mediators. *Trends in Biochemical Sciences*, *31*(2), 89–97. https://doi.org/10.1016/j.tibs.2005.12.008

Krause, B. J., Costello, P. M., Muñoz-Urrutia, E., Lillycrop, K. A., Hanson, M. A., & Casanello, P. (2013). Role of DNA methyltransferase 1 on the altered eNOS expression in human umbilical endothelium from intrauterine growth restricted fetuses. *Epigenetics*, *8*(9), 944–952. https://doi.org/10.4161/epi.25579

Krause, B. J., Hernandez, C., Caniuguir, A., Vasquez-Devaud, P., Carrasco-Wong, I., Uauy, R., & Casanello, P. (2016). Arginase-2 is cooperatively up-regulated by nitric oxide and histone deacetylase inhibition in human umbilical artery endothelial cells. *Biochemical Pharmacology*, *99*, 53–59. https://doi.org/10.1016/j.bcp.2015.10.018

Light, W. H., Freaney, J., Sood, V., Thompson, A., D'Urso, A., Horvath, C. M., & Brickner, J. H. (2013). A conserved role for human Nup98 in altering chromatin structure and promoting epigenetic transcriptional memory. *PLoS Biology*, *11*(3), e1001524. https://doi.org/10.1371/journal.pbio.1001524

Locigno, R., & Castronovo, V. (2001). Reduced glutathione system: Role in cancer development, prevention and treatment. *International Journal of Oncology*, https://doi.org/10.3892/ijo.19.2.221

Lowry, O. H., Rosebrogh, N. J., Farr, A. L., & Randall, R. J. (1951). Protein measurement with the Folin phenol reagent. *The Journal of Biological Chemistry*, *193*(1), 265–275.

Lushchak, V. I. (2010). Adaptive response to oxidative stress: Bacteria, fungi, plants and animals. *Comparative Biochemistry and Physiology, Part C*, *153*, 175–190. https://doi.org/10.1016/j.cbpc.2010.10.004

Ma, Q. (2013). Role of nrf2 in oxidative stress and toxicity. *Annual Review of Pharmacology and Toxicology*, *53*, 401–426. https://doi.org/10.1146/annurev-pharmtox-011112-140320

Malti, N., Merzouk, H., Merzouk, S. A., Loukidi, B., Karaouzene, N., Malti, A., & Narce, M. (2014). Oxidative stress and maternal obesity: Feto-placental unit interaction. *Placenta*, *35*(6), 411–416. https://doi.org/10.1016/j.placenta.2014.03.010

Mane, V. P., Heuer, M. A., Hillyer, P., Navarro, M. B., & Rabin, R. L. (2008). Systematic method for determining an ideal housekeeping gene for real-time PCR analysis. *Journal of Biomolecular Techniques*, *19*(5), 342–347. https://doi.org/10.1111/j.1750-3841.2008.00880.x

Marseglia, L., Manti, S., D'Angelo, G., Nicotera, A., Parisi, E., Di Rosa, G., & Arrigo, T. (2015). Oxidative stress in obesity: A critical component in human diseases. *International Journal of Molecular Sciences*, *16*(1), 378–400. https://doi.org/10.3390/ijms16010378

Martyn, K. D., Frederick, L. M., von Loehneysen, K., Dinauer, M. C., & Knaus, U. G. (2006). Functional analysis of Nox4 reveals unique characteristics compared to other NADPH oxidases. *Cellular Signalling*, *18*(1), 69–82. https://doi.org/10.1016/J.CELLSIG.2005.03.023

McMahon, M., Itoh, K., Yamamoto, M., & Hayes, J. D. (2003). Keap1-dependent proteasomal degradation of transcription factor Nrf2 contributes to the negative regulation of antioxidant response element-driven gene expression. *Journal of Biological Chemistry*, *278*(24), 21592–21600. https://doi.org/10.1074/jbc.M300931200

Mcmillen, I. C. (2005). Developmental origins of the metabolic syndrome: Prediction, plasticity, and programming. *Physiological Reviews*, *85*(2), 571–633. https://doi.org/10.1152/physrev.00053.2003

Milad, M. A., Novoa, J. M. P., Fabres, J. B., Margarita Samamé, M. M., Aspillaga, C. M., Rama de Neonatología, D., & Chilena de Pediatría, S. (2010). Recomendación sobre Curvas de Crecimiento Intrauterino. *Revista chilena de pediatría*, *81*(3), 264–274.

Miller, E. W., Dickinson, B. C., & Chang, C. J. (2010). Aquaporin-3 mediates hydrogen peroxide uptake to regulate downstream intracellular signaling. *Proceedings of the National Academy of Sciences*, *107*(36), 15681–15686. https://doi.org/10.1073/pnas.1005776107

Muñoz-Muñoz, E., Krause, B. J., Uauy, R., & Casanello, P. (2018). LGA-newborn from patients with pregestational obesity present reduced adiponectin-mediated vascular relaxation and endothelial dysfunction in fetoplacental arteries. *Journal of Cellular Physiology*, *233*(10), 6723–6733. https://doi.org/10.1002/jcp.26499

Nguyen, D., & Nguyen, D. (2013). Quantifying chromogen intensity in immunohistochemistry via reciprocal intensity. *Protocol Exchange*, https://doi.org/10.1038/protex.2013.097

Nguyen, T., Nioi, P., & Pickett, C. B. (2009). The Nrf2-antioxidant response element signaling pathway and its activation by oxidative stress. *The Journal of Biological Chemistry*, *284*(20), 13291–13295. https://doi.org/10.1074/jbc.R900010200

Nguyen, T., Sherratt, P. J., Huang, H. -C., Yang, C. S., & Pickett, C. B. (2003). Increased protein stability as a mechanism that enhances Nrf2-mediated transcriptional activation of the antioxidant response element. Degradation of Nrf2 by the 26 S proteasome. *The Journal of Biological Chemistry*, *278*(7), 4536–4541. https://doi.org/10.1074/jbc.M207293200

Nguyen, T., Sherratt, P. J., Nioi, P., Yang, C. S., & Pickett, C. B. (2005). Nrf2 controls constitutive and inducible expression of ARE-driven genes through a dynamic pathway involving nucleocytoplasmic shuttling by Keap1. *Journal of Biological Chemistry*, *280*(37), 32485–32492. https://doi.org/10.1074/jbc.M503074200

Noctor, G., & Foyer, C. H. (1998). ASCORBATE AND GLUTATHIONE: Keeping active oxygen under control. *Annual Review of Plant Physiology and Plant Molecular Biology*, *49*(1), 249–279. https://doi.org/10.1146/annurev.arplant.49.1.249

Oken, E., & Gillman, M. W. (2003). Fetal origins of obesity. *Obesity Research*, *11*(4), 496–506. https://doi.org/10.1038/oby.2003.69

Pfaffl, M. W. (2001). A new mathematical model for relative quantification in real-time RT-PCR. *Nucleic Acids Research*, *29*(9), e45–e45.

Pickering, A. M., Vojtovich, L., Tower, J., & A Davies, K. J. (2013). Oxidative stress adaptation with acute, chronic, and repeated stress. *Free Radical Biology & Medicine*, *55*, 109–118. https://doi.org/10.1016/j.freeradbiomed.2012.11.001

Reik, W. (2007). Stability and flexibility of epigenetic gene regulation in mammalian development. *Nature*, *447*(7143), 425–432. https://doi.org/10.1038/nature05918

Román, F., Urra, C., Porras, O., Pino, A. M., Rosen, C. J., & Rodríguez, J. P. (2017). Real-time H2 O2 measurements in bone marrow mesenchymal stem cells (MSCs) show increased antioxidant capacity in cells from osteoporotic women. *Journal of Cellular Biochemistry*, *118*(3), 585–593. https://doi.org/10.1002/jcb.25739

Rosso, P. (1985). A new chart to monitor weight gain during pregnancy. *American Journal of Clinical Nutrition*, *41*(3), 644–652.

Saker, M., Soulimane Mokhtari, N., Merzouk, S. A., Merzouk, H., Belarbi, B., & Narce, M. (2008). Oxidant and antioxidant status in mothers and their newborns according to birthweight. *European Journal of Obstetrics, Gynecology, and Reproductive Biology*, *141*(2), 95–99. https://doi.org/10.1016/j.ejogrb.2008.07.013

Schneider, D., Hernández, C., Farías, M., Uauy, R., Krause, B. J., & Casanello, P. (2015). Oxidative stress as common trait of endothelial dysfunction in chorionic arteries from fetuses with IUGR and LGA. *Placenta*, *36*(5), 552–558. https://doi.org/10.1016/j.placenta.2015.02.003

Stewart, A. F., Reik, A., & Schütz, G. (1991). A simpler and better method to cleave chromatin with DNase1 for hypersensitive site analyses. *Nucleic Acids Research*, *19*(11), 3157–3157. https://doi.org/10.1093/nar/19.11.3157

Stöcker, S., Maurer, M., Ruppert, T., & Dick, T. P. (2017). A role for 2-Cys peroxiredoxins in facilitating cytosolic protein thiol oxidation. *Nature Chemical Biology*, *14*(2), 148–155. https://doi.org/10.1038/nchembio.2536

How to cite this article: Carrasco-Wong I, Hernández C, Jara-Gutiérrez C, Porras O, Casanello P. Human umbilical artery endothelial cells from Large-for-Gestational-Age newborn have increased antioxidant efficiency and gene expression. *J Cell Physiol*. 2019;1–16. https://doi.org/10.1002/jcp.28494